Received 10 June 2026; accepted 24 June 2026. Date of publication 2 July 2026; date of current version 10 July 2026.
The review of this article was arranged by Associate Editor Nick Fletcher.
Digital Object Identifier 10.1109/OJIM.2026.3709475

Algorithmic Optimization of Star-Mesh Quantized Hall Resistance Networks for Bridge Sensitivity

GRETCHEN B. FERGUSON[1,2], ALBERT F. RIGOSI[2] (Member, IEEE), DOMINICK S. SCALETTA[3], DAVID B. NEWELL[2], AND DEAN G. JARRETT[2] (Fellow, IEEE)

[1]Auburn University, Auburn, AL 36832 USA
[2]National Institute of Standards and Technology (NIST), Gaithersburg, MD 20899 USA
[3]Mount San Jacinto College, Menifee, CA 92584 USA

CORRESPONDING AUTHOR: D. G. JARRETT (dean.jarrett@nist.gov)

ABSTRACT Contemporary advances in electrical metrology include the understanding and development of star-mesh transformations and their applicability to the access of very high quantized resistances. These pursuits seek to drastically reduce the traceability chain for global calibrations, as demonstrated by a recent exemplary 1 GΩ star-mesh graphene quantized Hall array resistance standard (QHARS) using a dual-source bridge. Such studies revealed that there are limitations to many symmetrically iterated star-mesh devices, mainly due to single elements experiencing high enough current that its QHE breaks down, as well as general decreased bridge sensitivity. These two issues may be overcome by modifying the star-mesh designs to include a sufficient number of Hall elements at the first and last branches of the QHARS. In this work, new designs that give consideration to quantum Hall breakdown currents and bridge measurement performances were analyzed using the LTspice circuit simulator replicating the behavior of star-mesh devices in the quantized state. Several improved QHARS device designs for the outputs of 1 and 10 GΩ are reported, with most device output resistances falling within 500 $\mu\Omega/\Omega$ of nominal.

INDEX TERMS Calibration, electrical resistance measurement, quantum Hall effect, resistance, standards.

I. INTRODUCTION

THE quantized Hall array resistance standards (QHARS) are devices that accommodate many elements, each conventionally realizing a resistance that is a multiple of h/e^2, with h and e being the Planck constant and the elementary charge, respectively. Until the last decade, QHARS devices were fabricated almost exclusively using GaAs/AlGaAs heterostructures, after which epitaxial graphene (EG) emerged as a highly promising alternative for primary electrical metrology applications [1], [2]. While the global metrological community is in an ongoing state of transition rather than a complete, sudden replacement of GaAs-based standards, as highlighted by recent milestones, such as high-precision bilateral resistance comparisons utilizing graphene standards [3], [4], the adoption of graphene has grown rapidly due to its more user-friendly operating conditions [3], [5], [6], [7], [8], [9], [10], [11], [12], with many worldwide pursuits utilizing EG as a quantized Hall resistance (QHR) standard operating at the resistance plateau formed by the $i = 2$ Landau level (about half of the von Klitzing constant, or $R_H \approx 12\,906.4037\ \Omega$). Other plateaus, such as the $i = 6$ plateau, are considerably more difficult to access and are thus not subject to heavy use in metrology [13].

Traditional resistance scaling via QHARS devices typically encounters strict physical and geometric limitations beyond the MΩ level due to the complex fabrication requirements needed to link thousands of elements in series. Ever since the formalism of optimizing QHARSs by implementing recursive star-mesh transformations, metrologists have been able to access at least several quantized resistance values for calibration purposes [14], [15], [16]. In short, star-mesh transformations can be represented as a mathematical equivalence between a complex array of interconnected quantized Hall elements and a single, high-value resistor; furthermore, using the transformation in device design offers immense promise for bypassing the complexities of traditional resistance scaling.

This design simplification scheme (star-mesh QHARS device designs) also offers fabrication relief for values beyond the MΩ level, mainly by using recursive and multistage designs that drastically reduce the total number of required Hall elements needed for achieving very high resistances, hypothetically including those up to 1 EΩ [14].

Although star-mesh transformations provide potentially improved scaling methods by mathematically compounding resistance through complex multiterminal networks, conventional designs need algorithms that optimize solely for minimum element count without factoring in infrastructure compatibility, such as bridge sensitivity and internal current distributions.

The limitations of breakdown current and bridge sensitivity on symmetrically recursive star-mesh designs prompted the main messages of this work, which proposes a transition to asymmetric star-mesh networks to transcend those limitations. Simulations were performed that included high input voltages ranging from 20 to 100 V to test the bridge compatibility (sensitivity and breakdown current) of new designs for 1 and 10 GΩ QHARS devices.

Accompanying measurements are made on room-temperature resistance network assemblies to prove the concept of using asymmetric star-mesh designs. Although these new designs increase the element count by nearly a factor of two in the asymmetric case, the tradeoff is numerically justified by an assessment of dozens of configurations' Laplacian matrices, indicating that the networks of adequate electrical connectivity can still lead to heavy improvements in bridge sensitivity and higher test voltages, marking a crucial step forward in the pursuit to have graphene-based resistance standards replace conventional traceability chains to resistances above 1 MΩ.

II. LIMITATIONS OF SYMMETRICALLY RECURSIVE STAR-MESH DEVICES

A. SYMMETRICALLY RECURSIVE DEVICE DESIGNS

To substantially reduce the traceability chain, it is crucial to fabricate devices that can output quantized resistances much greater than the conventional value R_H. For example, creating a 10-GΩ QHARS in-series design would require about 7.75×10^5 elements, a number that is not feasible given the constraints of the element size and EG growth areas (which presently accommodate up to about 500 elements). However, using QHARS designs that leverage star-mesh transformations transcend this barrier [17], [18], allowing one to significantly decrease the number of elements to mere hundreds [14]. Following the general optimization procedures, one can obtain the device designs in Fig. 1(a)–(d), where one should note that the numbers adjacent to each resistance symbol are the coefficients of effective resistance (CERs) of R_H, sometimes used to normalize resistance to the value of the QHR [14].

Despite the low element count for these designs, incorporating these QHARS devices with other metrological infrastructure, like Wheatstone bridges, proves difficult due to the issues of breakdown current and bridge sensitivity. For instance, when these devices are wired in a similar fashion to those in [16], these symmetric devices often have current distributions that are more likely to result in branch or element breakdown (i.e., no longer sufficiently quantized). Breakdown has typically been observed at 12 V for a 1-GΩ

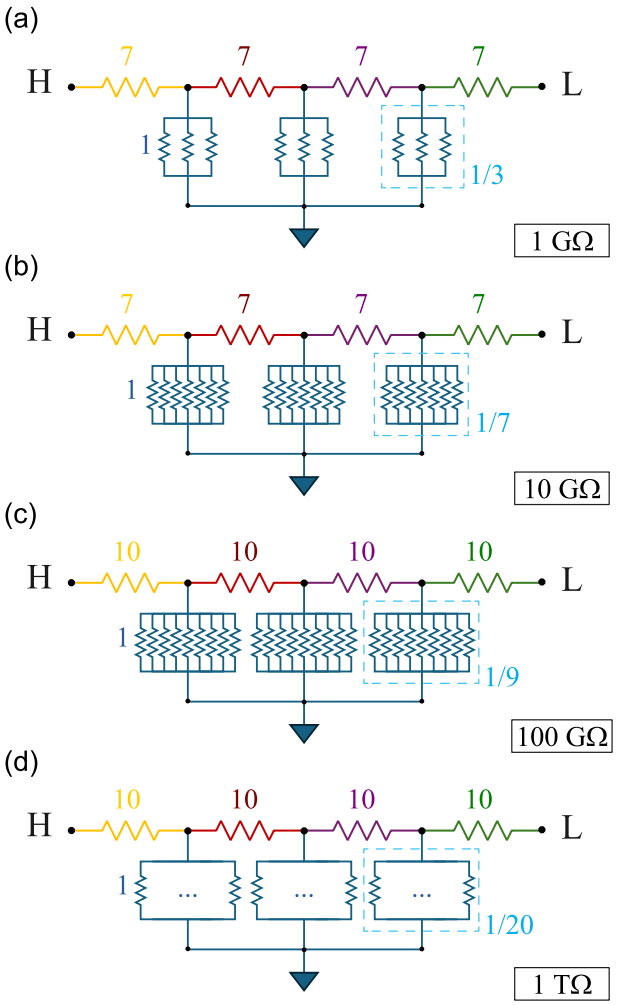

FIGURE 1. Symmetrically recursive star-mesh configuration for QHARS device designs with the following approximate outputs. (a) 1 GΩ, (b) 10 GΩ, (c) 100 GΩ, and (d) 1 TΩ. These designs found by optimizing element count substantially reduce what would have been required of an in-series design. The numbers adjacent to a resistor symbol are CERs of R_H, frequently used to normalize resistance to the value of the QHR.

QHARS [16]. For that reason, the simulations of symmetric star-mesh designs did not use voltages beyond 20 V. Table 1 shows the predicted values ranging from 1 GΩ to 1 TΩ and hypothetically designable with symmetric recursion. One note to make about the bridge sensitivities in Table 1 is that they decrease rapidly with increasing resistance, and low sensitivities typically translate to diminished detection of changes in the circuit. For context, the sensitivity of the first column (1 GΩ) approximately reflects the performance reported in [16], whose uncertainties were at or better than those used in calibrations. Departing from these sensitivities by orders of magnitude may result in measurements with larger uncertainties.

B. ASYMMETRIC DEVICE DESIGN CONSIDERATIONS

With the problem of compatibility between these star-mesh QHARS devices and bridge infrastructure defined, solutions

TABLE 1. Symmetric Star-Mesh Design Corresponding Device Parameters.

Devices	1 GΩ	10 GΩ	100 GΩ	1 TΩ
Resistance (GΩ)	1.095070	11.9751	100.477	1.06374
Correction (μΩ/Ω)	95069.6	197512	4767.62	63744.9
Number of elements	37	49	67	100
Critical applied voltage (V)	20	20	20	20
Critical current (μA)	211.731	217.032	153.277	154.195
Approximate Sensitivity (μV/V)	86.4	7.70	1.30	0.122

Description of parameters associated with four different QHARS designs adopting a symmetric, recursive star-mesh configuration, with values ranging 1 GΩ to 1 TΩ. The equivalent resistance is shown with a corresponding correction to the nearest nominal decade value. Each design also enumerates the total number of Hall elements, a hypothetically applicable voltage, a critical current (i.e. the maximum current experienced by an element in the array, whose knowledge is crucial to know for quantum Hall breakdown), and approximated bridge sensitivity per Equation 1.

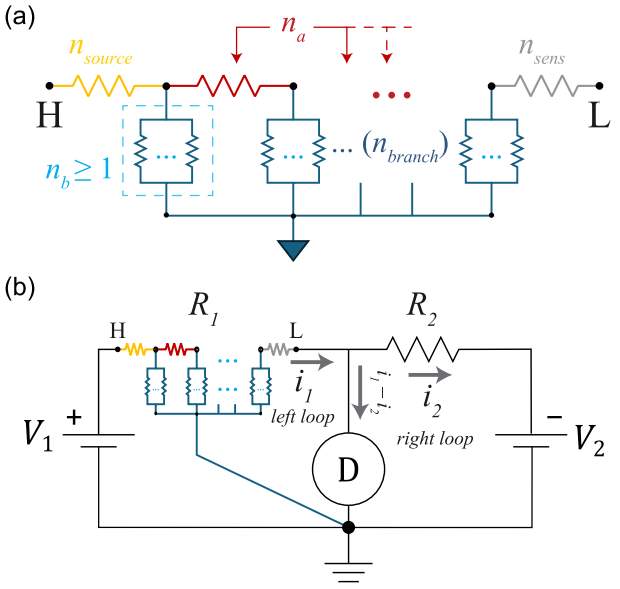

FIGURE 2. (a) Star-mesh configuration for a future QHARS device design is parameterized using five variables: 1) the number of elements in the first branch (n_{source}); 2) the number of elements in the final branch (n_{sens}); 3) the number of rungs in the ladder when viewing the circuit as a series-parallel ladder (n_{branch}); and 4) and 5) the number of series (n_a) and parallel (n_b) elements within each leg between nodes. In a symmetrically recursive star-mesh device, the yellow, red, and gray segments between nodes are always equal. "H" and "L" refer to the high- and low-voltage potentials, respectively. (b) Circuit diagram of the DSB showing how the asymmetric star-mesh device is incorporated.

were explored for keeping the massive benefit of accessing high quantized resistances and ensuring that such devices can be adequately measured. To overcome this issue, asymmetric designs were algorithmically determined, whereby the resistance of the first and last branches of any star-mesh design was increased to a number of elements necessary to enable higher voltages for resistance measurements without breaking down device quantization [see Fig. 2(a)].

The measurement performance of the design was evaluated with the help of the LTspice circuit simulator (see commercial disclaimer). More details on this overall algorithm are in Section III-A, and the resulting device modifications aimed to accommodate an increased breakdown current threshold of the overall device. The connectivity of these asymmetric designs was later quantified with weighted Laplacian matrices and compared with symmetric counterparts to validate the notion that a lower element count is still the primary parameter being optimized despite the new experimental constraints.

An intuitive qualitative analysis of these networks reveals a fundamental tradeoff between structural complexity and performance. In a traditional three-terminal resistance measurement, resistance amplification is achieved by shunting a fraction of the input current to the ground terminal rather than the low-potential terminal. The less current that is shunted to ground, the smaller the current experienced by the most vulnerable device (typically adjacent to the high terminal), thereby raising the maximum applicable measurement voltage before quantum Hall breakdown occurs.

Concurrently, minimizing this ground shunt limits the degree to which the detector path is loaded, inherently preserving a higher bridge sensitivity. The critical tradeoff, therefore, lies in balancing these infrastructure benefits against fabrication feasibility. Optimizing the network to withstand higher voltages and to maximize bridge sensitivity requires placing a significantly larger number of elements in series between the high and low nodes, which may nearly double the device element count and complicate device fabrication.

III. METHODOLOGY

A. ALGORITHMIC OPTIMIZATION

The MATLAB code (see commercial disclaimer) was written to facilitate an algorithmic process for designing high-resistance QHARS devices in the GΩ range. Since R_H (about 12 906.4037 Ω) is much smaller than 1 and 10 GΩ, one may use a specific network topology that modifies the symmetrically recursive star-mesh network, mainly by introducing asymmetries, to scale that resistance up significantly. One may list all configurations of elements in the neighborhood of the element count minimum to reach the target values of 1 and 10 GΩ with little deviation from the target being a parametric constraint.

The core objective of the code is to check thousands of possible circuit configurations, varying the following parameters, as seen in Fig. 2(a): 1) n_{source} (number of elements in the first branch); 2) n_{sens} (number of elements in the final branch); 3) n_{branch} (number of stages/rungs in the ladder when viewing the circuit as a series–parallel ladder); and 4) n_a and n_b [number of elements within each segment between nodes; n_a for those segments containing only in-series elements (red) and n_b for those segments containing only in-parallel elements (within each dark blue branch)]. For each combination tested, the equivalent resistance gets calculated, and the value is compared to the relevant target value (1 or 10 GΩ). If the difference (correction) is less

than 1%, the configuration is saved. Finally, the code was written to track various parameters like those seen in Table 1 [i.e., the total resistance of the new design (n_{tot}), the correction from the target values, and the total number of elements in a device (D_T)].

B. DUAL-SOURCE BRIDGE

To validate the concept of designing asymmetric star-mesh networks for eventual EG-based QHARS devices, example measurements were performed using a dual-source bridge (DSB). Also known as a modified Wheatstone bridge, this apparatus has been used at several National Metrology Institutes [19], [20], [21], [22]. The bridge functions by means of applying voltage V_1 across a reference resistance R_1. A second source simultaneously applies a voltage V_2 (of opposite polarity) across an unknown resistor R_2. The quantities R_1 or R_2 may be in either arm since the voltage sources are typically interchangeable. A schematic of the bridge is illustrated in Fig. 2(b). The two voltage sources (V_1 and V_2) are two calibrators (Fluke 5730A and 5720A, see commercial disclaimer). The sources were calibrated using an automated potentiometer based on a Cutkosky binary voltage divider [23], and the detector was a 7.5-digit digital nanovoltmeter (Keysight 34420A, see disclaimer). The low sides of the two calibrators and the detector are connected to a common ground. The measurement sequence is well summarized in [16].

One substantial advantage gained by using a DSB is the low uncertainties that may be obtained because of the relatively simple calibration of the voltage sources. Moreover, the effects from leakage become negligible because the bridge detector, which has a high level of sensitivity, becomes balanced with a null current and the low impedance ($< 0.1\ \Omega$ at DC) of the voltage sources. The uncertainties therefore originate from the calibration of the voltage sources, electrical noise, offset voltages, and R_S.

IV. RESULTS AND DISCUSSION

A. APPLYING THE ALGORITHM—NEW QHARS DEVICES

To evaluate the feasibility of balancing these networks with a DSB, one defines bridge sensitivity as the change in detector voltage (V_D) per unit change in the unknown network resistance (R_1). This metric directly determines the experimental signal-to-noise floor during high-resistance calibrations. Looking at the primary current paths within the dual-source configuration depicted in Fig. 2(b), the sensitivity can be mathematically derived by analyzing small voltage perturbations across the shared path of the largest left and right loops

$$\frac{\partial V_D}{\partial R_2} = \frac{\partial}{\partial R_1}\left\{V_{sens} + \left[V_{b(1)} + \left(V_{a(1)} + \ldots\right)^{-1}\right]^{-1}\right\}. \quad (1)$$

Equation (1) describes how perturbations in R_1 propagate to the detector terminal through the partial derivatives of the branch networks. As briefly described in Section III, the parameter n_a dictates the series resistance components (R_a) forming the main horizontal rungs of the series–parallel ladder, whereas n_b determines the parallel components (R_b) within each grounded branch. Because the overall effective resistance of the low-side branch (R_{sens}) must remain large to accommodate elevated voltages, one may approximate $R_{sens} \gg R_a$. Consequently, the derivative reveals that the bridge sensitivity is most heavily dependent on a summation of R_{sens} and $R_{b(1)}$ (the nearest adjacent grounded branch).

Therefore, (1) allows one to take promising asymmetric designs and determine whether they are feasible to measure with a DSB. The results for four exemplary designs (1 and 10 GΩ) are summarized in Table 2.

TABLE 2. Asymmetric Star-Mesh Design Corresponding Device Parameters.

Devices	Original Symmetric Star-Mesh	1 GΩ (A)	1 GΩ (B)	10 GΩ (A)	10 GΩ (B)
Resistance (GΩ)	1.095070	0.999627	1.00044	9.991712	10.00017
Correction (μΩ/Ω)	95069.6	373.2	439.9	828.8	16.6
Number of elements (D_T)	37	64	68	71	74
Critical applied voltage (V)	20	100	100	100	100
Critical current (μA)	211.731	239.389	298.968	212.646	259.755
Sensitivity (μV/V)	86.2	276	270	28.2	27.7

Description of parameters associated with four different QHARS designs adopting an asymmetric star-mesh configuration, two designs being valued near 1 GΩ and the other two near 10 GΩ. The equivalent resistance is shown with a corresponding correction to the nearest nominal decade value. Each design also enumerates the total number of Hall elements, a hypothetically applicable voltage, a critical current, and improvement to the bridge sensitivity.

From Table 2, one can design new devices, like the one in Fig. 3(a), which shows a lithographic mask for fabricating a 10 GΩ (B) QHARS device. With the corresponding schematic in Fig. 3(b), one may also calculate important quantities like the critical current and the expected bridge sensitivity when utilizing this device.

A comparison between Tables 1 and 2 highlights an important topological distinction regarding performance. Within a fixed circuit configuration, such as the symmetric topology in Table 1, increasing the nominal resistance target from 1 to 10 GΩ drastically degrades the approximate bridge sensitivity from 86.4 μV/V down to 7.70 μV/V. This degradation is reversed in Table 2, where the asymmetric 10 GΩ configurations achieve the elevated sensitivities of 28.2 μV/V (Design A) and 27.7 μV/V (Design B). It should be noted that this apparent sensitivity enhancement (comparing the 10 GΩ asymmetric to symmetric cases) is a mathematical consequence of transitioning from a symmetric recursive structure to an algorithmically optimized asymmetric topology.

B. PROOF OF CONCEPT WITH ARTIFACT RESISTOR NETWORKS

With asymmetric device designs that now allow for better bridge sensitivity, the next step to proving the concept prior to embarking on a time-consuming fabrication pursuit is to

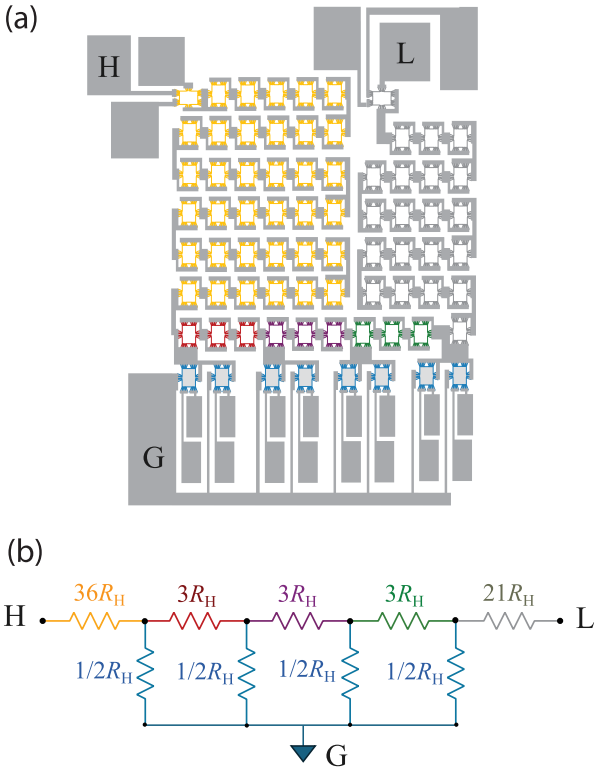

FIGURE 3. (a) Asymmetric star-mesh configuration for a QHARS device divided into color-coded segments. Although the optimization algorithm from [14] yielded a total number of 37 quantum Hall elements (for a symmetrically recursive star-mesh QHARS device that outputs approximately 1 GΩ), constraints on the ability to measure such a device with a DSB necessitate the implementation of twice as many elements. This is a proposed lithographic mask intended for fabricating the first asymmetric star-mesh graphene-based QHARS device [see Table 2, 10 GΩ (B)]. (b) Schematic of the circuit diagram indicates the exact number of quantum Hall elements needed in each segment and matches the color-coding scheme in (a) (with a total of 74 elements). "H" and "L" refer to the high- and low-voltage potentials, respectively.

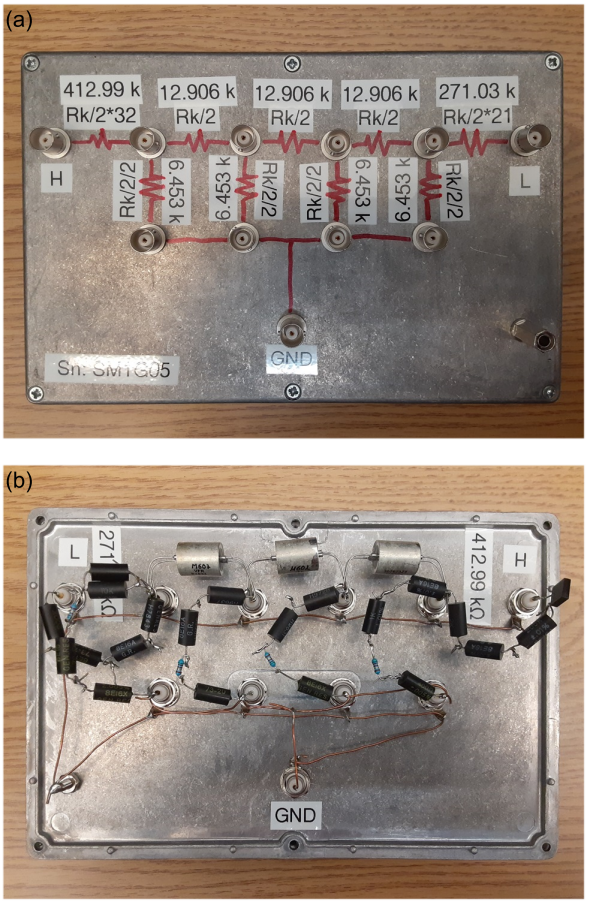

FIGURE 4. Resistor network using the asymmetric star-mesh design obtained during algorithmic optimization. (a) External appearance of the artifact emulating the new, asymmetric star-mesh design with visual aids drawn on. (b) Internal appearance with visual aids.

emulate a real network and to measure it accordingly. Two artifact networks were built with similar component resistors, one emulating the original symmetrically recursive star-mesh network (first column of Table 2) and the other emulating the new, asymmetric star-mesh network (second column of Table 2). Fig. 4(a) and (b) shows the asymmetric artifact resistor network meant to emulate the second column of Table 2.

When both networks underwent measurements with the DSB, there was a substantial difference between each network and its predicted value (see the gold dashed lines in Fig. 5). Fig. 5(a) and (b) has identical vertical scales, with the inset of the symmetric network needed to convey the larger offset from the network's predicted value. Three distinct ratios were measured, requiring three separate resistance standards (1 GΩ, 100 MΩ, and 10 GΩ), whose corresponding data are in black, red, and light blue, respectively. One key observation to make is that the spread of the data is greater in the symmetric network, which is aligned with the lower computed bridge sensitivity compared to the asymmetric network.

It is also important to emphasize that because these networks were created using commercial resistors as opposed to EG-based QHARS devices, the absolute proximity of the data to the true predicted value in both cases Fig. 5(a) and (b) is an artifact of the physical assembly rather than an intrinsic feature of the asymmetric design. Therefore, the primary indicator of enhanced measurement performance must be evaluated through the data dispersion (spread) across the various measurement ratios.

For Fig. 5(a), the artifact network had a predicted value of 1.095070 GΩ and, when incorporated with the DSB, resulted in a computed bridge sensitivity of about 86 μV/V. The symmetric network yielded a larger data spread across each of the three ratios, specifically by more than a factor of 3 when compared with Fig. 5(b) (asymmetric). The asymmetric star-mesh design (based on the "A" case in Table 2, but being an imperfect resistor network with a value very slightly different than that of the QHARS value of 0.999627 GΩ), having a predicted value of 1.000590 GΩ when all components were measured with a multimeter (Keysight 3458A, see disclaimer), had a higher computed bridge sensitivity of about 276 μV/V and consequently showed a tighter data grouping. This marked reduction in statistical dispersion demonstrates

that the asymmetric framework can lead to improved bridge sensitivity achievable with a corresponding QHARS device.

C. FURTHER NUMERICAL SUPPORT FROM THE LAPLACIAN MATRIX

While direct inspection of a design easily demonstrates that the element directly adjacent to the high potential terminal bears the greatest current load and breakdown risk, evaluating a network solely in this way is insufficient for complex multielement arrays. One may introduce the weighted Laplacian matrix to serve as a global structural health check for the QHARS. This matrix approach helps clarify that a device designer has not unintentionally introduced secondary current bottlenecks elsewhere in the array. One example of a secondary current bottleneck is a single Hall element along one rung or branch in the array, whose placement may not be obvious if QHARS design parameters are determined algorithmically (as with an automated program that outputs the parameters described in Section III-A). Such bottlenecks mathematically reduce the connectivity quantified by this matrix.

One of the key benefits of using the symmetrically recursive star-mesh designs was the ability to maintain large connectivity throughout the device. To further support the notion that asymmetric designs can be used without compromising this connectivity, one may more explicitly quantify this property by using the aforementioned weighted Laplacian matrix, which is a positive, semi-definite matrix in spectral graph theory that conveys the interconnectedness of a network. The matrix itself may be intuited to be the discretized Laplace operator. In conventional calculus, the Laplace operator (∇^2) measures the difference between the value of a function at a point and the average value of the function around that point. The Laplacian matrix measures the difference between a node's value and the average of its neighbors, and it is defined to be

$$L_G := G_{i,j} = \begin{pmatrix} G_{1,1} & \cdots & G_{1,N} \\ \vdots & \ddots & \vdots \\ G_{N,i} & \cdots & G_{N,N} \end{pmatrix}$$

$$G_{i,j} = \begin{cases} G_{i,i}; & \text{if } i = j \\ -G_a; & \text{if } |i-j| = 1 \\ 0; & \text{otherwise} \end{cases} \quad (2)$$

and

$$G_{i,i} = G_b + \left(2 - \delta_{i,1} - \delta_{i,N}\right) G_a + \delta_{i,1} G_{source} + \delta_{i,N} G_{sens} \quad (3)$$

In (2) and (3), G is the conductivity of a segment, with identical subscripts to Fig. 2(a), $N = n_{branch} = n_a - 1$, and δ is the Kronecker delta. Specifically, each entry in the matrix is the reciprocal of the corresponding resistance for that segment since L_G is intuitively representing connectedness (i.e., conductivity).

By taking the determinant of (2) ($det(L_G)$), one quantifies the connectedness of a network. Again, this type of assessment is important to consider because a poorly connected network may inevitably lead to similar concerns of electrical current overloading sections of a QHARS to the point of breakdown of quantization. For each of the dozens of design combinations found with the MATLAB code for the 1 GΩ case (and dozens more for the 10 GΩ case), a weighted Laplacian matrix was created and its determinant calculated. These determinants are plotted as a function of D_T (a quantity that remains static) and shown in Fig. 6.

One key takeaway is that, even though symmetrically recursive star-mesh Laplacian matrices yield determinants [red data point in Fig. 6(a) and (b) insets] that are more optimal in terms of both connectedness and element count, the determinants seen in asymmetric cases are not so drastically smaller relative to the range of the set of designs, and although one cannot anticipate the successful fabrication of asymmetric network resistances using QHARS based on this determinant alone, the value can indicate if a design is likely to contain secondary bottlenecks, such as the earlier example of a single Hall element along a single rung of the ladder. Such current bottlenecks should be avoided since a single-element failure would cause greater measurement deviations.

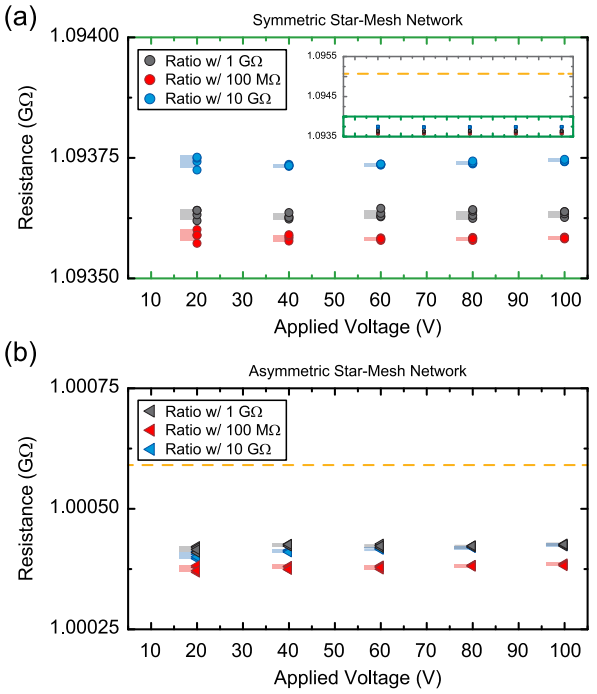

FIGURE 5. DSB data were collected for two artifact networks with values near 1 GΩ but based on different network design approaches. In both cases, three separate ratios were measured (requiring three different standards): a 1:1 ratio with a 1-GΩ resistor (black), a 10:1 ratio with a 100-MΩ resistor (red), and a 1:10 ratio with a 10-GΩ resistor (light blue). Both panels' vertical scales are identical in increment. The shaded regions that are adjacent to data points on their left denote the combined standard uncertainty associated with measurements at each ratio. (a) Data from a symmetrically recursive star-mesh design, which seeks to solely minimize the element count of a future QHARS device. This artifact network has a predicted value of 1.095070 GΩ and, when incorporated with the DSB, has a lower computed bridge sensitivity (resulting in a greater spread of the data compared to the next case). (b) Data from an asymmetric star-mesh design, which seeks to balance a low element count with DSB compatibility. This artifact network has a predicted value of 1.000590 GΩ and, when incorporated with the DSB, has a higher computed bridge sensitivity (resulting in a smaller spread of the data). The gold dashed lines in both panels indicate the predicted value of the artifact resistor network [necessitating a zoom-out inset in (a), with a green set of axes representing the main panel axes].

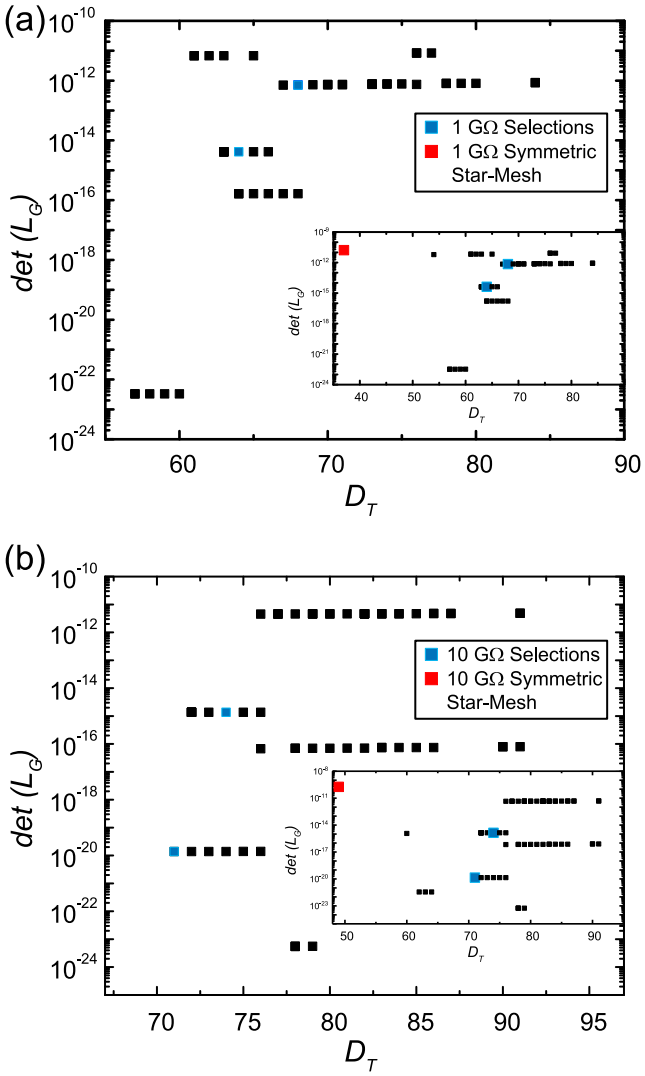

FIGURE 6. Scatterplots are provided for the determinants of weighted Laplacian matrices against the total element count (D_T) of the corresponding simulated device configurations. Designs for (a) 1 and (b) 10 GΩ are assessed, with light blue data points (two per panel) correspond to the two selected designs for each value as stated in Table 2. Each panel contains an inset that provides a full picture of the same scatterplot (with data points of interest enlarged) including the assessment of the symmetrically recursive star-mesh design (first two columns of Table 1).

Lastly, observing a reduction in mathematical connectivity (det(L_G)) does not justify rejecting a design, especially since there are immense practical gains to be obtained in bridge sensitivity and voltage tolerance. However, observing too low a value relative to the range of a set of designs does indicate a need to carefully inspect corresponding designs for secondary or tertiary bottlenecks for electrical current. Future investigations may explore how star-mesh designs for other values of quantized resistance differ when comparing symmetric and asymmetric configurations.

V. CONCLUSION

Overall, this work begins with the supposition that symmetrically recursive star-mesh QHARS designs successfully minimize element counts but are often incompatible with metrological infrastructure due to breakdown currents of the quantum Hall effect and insufficient bridge sensitivity. It is then demonstrated that by transitioning to algorithmically determined asymmetric star-mesh designs, one may redistribute internal potentials to support higher test voltages and significantly enhanced bridge sensitivity at the 1 and 10 GΩ levels. Although these asymmetric configurations nearly double the required element count, Laplacian matrix assessments and room-temperature network measurements confirm that the designs maintain high electrical connectivity and near-optimal element count. These advancements will enable EG-based QHARS to replace conventional traceability chains for resistances exceeding 1 MΩ.

ACKNOWLEDGMENT

The authors thank S. Schlamminger, N. T. M. Tran, Y. Yang, and A. R. Panna for their fruitful discussions. Work presented herein was performed, for a subset of the authors, as part of their official duties for U.S. Government. Funding is hence appropriated by U.S. Congress directly. Commercial equipment, instruments, and materials are identified in this article in order to specify the experimental procedure adequately. Such identification is not intended to imply recommendation or endorsement by the National Institute of Standards and Technology or U.S. Government, nor is it intended to imply that the materials or equipment identified are necessarily the best available for the purpose.

REFERENCES

[1] T. J. B. M. Janssen et al., "Precision comparison of the quantum Hall effect in graphene and gallium arsenide," *Metrologia*, vol. 49, no. 3, pp. 294–306, Jun. 2012.

[2] J. Kucera, P. Svoboda, and K. Pierz, "AC and DC quantum Hall measurements in GaAs-based devices at temperatures up to 4.2 k," *IEEE Trans. Instrum. Meas.*, vol. 68, no. 6, pp. 2106–2112, Jun. 2019.

[3] T. Oe et al., "Comparison between NIST graphene and AIST GaAs quantized Hall devices," *IEEE Trans. Instrum. Meas.*, vol. 69, no. 6, pp. 3103–3108, Jun. 2020.

[4] P. Gournay, B. Rolland, M. Kruskopf, J. Lengsfeld, and D. K. Patel, "On-site comparison of quantum Hall effect resistance standards of the PTB and the BIPM: Ongoing key comparison BIPM.EM-K12," *Metrologia*, vol. 62, no. 1A, p. 1010, Jan. 2025.

[5] M. Kruskopf et al., "Next-generation crossover-free quantum Hall arrays with superconducting interconnections," *Metrologia*, vol. 56, no. 6, Dec. 2019, Art. no. 065002.

[6] M. Kruskopf et al., "Two-terminal and multi-terminal designs for next-generation quantized Hall resistance standards: Contact material and geometry," *IEEE Trans. Electron Devices*, vol. 66, no. 9, pp. 3973–3977, Sep. 2019.

[7] A. Lartsev, S. Lara-Avila, A. Danilov, S. Kubatkin, A. Tzalenchuk, and R. Yakimova, "A prototype of RK/200 quantum Hall array resistance standard on epitaxial graphene," *J. Appl. Phys.*, vol. 118, no. 4, Jul. 2015, Art. no. 044506.

[8] S. Novikov et al., "Mini array of quantum Hall devices based on epitaxial graphene," *J. Appl. Phys.*, vol. 119, no. 17, May 2016, Art. no. 174504.

[9] J. Park, W.-S. Kim, and D.-H. Chae, "Realization of $5\frac{h}{e^2}$ with graphene quantum Hall resistance array," *Appl. Phys. Lett.*, vol. 116, no. 9, Mar. 2020, Art. no. 093102.

[10] H. He et al., "Accurate graphene quantum Hall arrays for the new international system of units," *Nature Commun.*, vol. 13, no. 1, p. 6933, Nov. 2022.

[11] A. Tzalenchuk et al., "Towards a quantum resistance standard based on epitaxial graphene," *Nature Nanotechnol.*, vol. 5, no. 3, pp. 186–189, Mar. 2010.

[12] M. Woszczyna et al., "Precision quantization of Hall resistance in transferred graphene," *Appl. Phys. Lett.*, vol. 100, no. 16, Apr. 2012, Art. no. 164106.
[13] A. R. Panna et al., "Graphene quantum Hall effect parallel resistance arrays," *Phys. Rev. B, Condens. Matter*, vol. 103, Feb. 2021, Art. no. 075408.
[14] D. S. Scaletta et al., "Optimization of graphene-based quantum Hall arrays for recursive star–mesh transformations," *Appl. Phys. Lett.*, vol. 123, no. 15, Oct. 2023, Art. no. 153504.
[15] D. G. Jarrett et al., "Graphene-based star–mesh resistance networks," *IEEE Trans. Instrum. Meas.*, vol. 72, pp. 1–10, 2023.
[16] M. Musso et al., "Implementation of a 1 GΩ star-mesh graphene quantized Hall array resistance standard network for high resistance calibration," *IEEE Trans. Instrum. Meas.*, vol. 74, pp. 1–12, 2025.
[17] A. E. Kennelly, "Equivalence of triangles and stars in conducting networks," *Elect. World Engineer*, vol. 34, pp. 413–414, Jan. 1899.
[18] L. Versfeld, "Remarks on star-mesh transformation of electrical networks," *Electron. Lett.*, vol. 6, no. 19, pp. 597–599, Sep. 1970.
[19] D. G. Jarrett, "Automated guarded bridge for calibration of a multimegohm standard resistors from 10MΩ to 1 TΩ" *IEEE Trans. Instrum. Meas.*, vol. 46, pp. 325–328, 1997.
[20] D. G. Jarrett et al., "Graphene quantized Hall arrays as wye-delta transfer standards," in *Proc. Conf. Precis. Electromagn. Meas. (CPEM)*, 2023, pp. 1–2.
[21] L. C. A. Henderson, "A new technique for the automatic measurement of high value resistors," *J. Phys. E, Sci. Instrum.*, vol. 20, no. 5, pp. 492–495, May 1987.
[22] G. Rietveld, D. Jarrett, and B. Jeckelmann, "Accurate high-ohmic resistance measurement techniques up to 1 PO," in *Proc. 29th Conf. Precis. Electromagn. Meas. (CPEM)*, Aug. 2014, pp. 290–291.
[23] R. D. Cutkosky, "A new switching technique for binary resistive dividers," *IEEE Trans. Instrum. Meas.*, vol. IM-27, no. 4, pp. 421–422, Dec. 1978.

GRETCHEN B. FERGUSON was born in Las Vegas, NV, USA. She is currently pursuing the bachelor's degrees in physics and mathematics with Auburn University, Auburn, AL, USA.

In early 2026, she began collaborating with the National Institute of Standards and Technology (NIST), Gaithersburg, MD, USA.

Ms. Ferguson was awarded a Summer Undergraduate Research Fellowship for Summer 2026.

ALBERT F. RIGOSI (Member, IEEE) was born in New York, NY, USA. He received the B.A., M.A., M.Phil., and Ph.D. degrees in physics from Columbia University, New York.

From 2008 to 2015, he was a Research Assistant with Columbia Nano Initiative, New York. From 2015 to 2016, he was a Joint Visiting Research Scholar with the Department of Applied Physics, Stanford University, Stanford, CA, USA, and the PULSE Institute, SLAC National Accelerator Laboratory, Menlo Park, CA, USA. Since 2016, he has been a Physicist with the National Institute of Standards and Technology, Gaithersburg, MD, USA. His research interests include 2-D electron systems and applications of those systems' behaviors for electrical metrology.

Dr. Rigosi is a member of American Physical Society and the Advisory Board for the Industrial Leadership in Physics Ph.D. Program at Georgetown University. He was awarded Associateships and Fellowships from the National Research Council, USA, the Optical Society of America, the Ford Foundation, and the National Science Foundation (Graduate Research Fellowship Program).

DOMINICK S. SCALETTA was born in Chicago, IL, USA. He received the B.S. degree in physics and the B.A. degree in mathematics from Columbia University, New York, NY, USA, and the M.S. degree in mathematics at the University of California, Riverside, Riverside, CA, USA.

He is currently a Professor of mathematics and physics and the Chair of the Department of Physics and Astronomy, Mount San Jacinto College, Menifee, CA, USA. His interests are in mathematical physics with the key focus on Feynman's path integral and its relationship to quantum groups, as well as the quantum Hall effect and its remarkable relationship with geometry and topology.

DAVID B. NEWELL received the B.S. degree in physics and the B.A. degree in mathematics from the University of Washington, Seattle, WA, USA, and the Ph.D. degree in physics from the University of Colorado, Boulder, CO, USA.

He was awarded the NRC Post-Doctoral fellowship to work on the Watt Balance Project at the National Institute of Standards and Technology (NIST), Gaithersburg, MD, USA, and became a full-time Staff Member in 1996. He has worked on measurements for realizing micro and nanoscale forces traceable to the SI, was the Leader of the Fundamental Electrical Measurements (FEM) Group, NIST, from 2004 to 2010, helped establish the use of graphene in quantum electrical standards, worked with a NIST team to construct a new watt balance to realize the kilogram from a fixed value of the Planck constant, and, as the Chair of the CODATA Task Group on Fundamental Constants, provided the exact values of the fundamental constants to be used in the new SI. He has presently again accepted responsibility as the Leader of the FEM group.

Dr. Newell is a member of the Philosophical Society of Washington, the Chair for the CODATA Task Group on Fundamental constants, and a fellow of the American Physical Society.

DEAN G. JARRETT (Fellow, IEEE) was born in Baltimore, MD, USA, in 1967. He received the B.S. degree in electrical engineering from the University of Maryland, College Park, MD, USA, in 1990, and the dual M.S. degree in electrical engineering and applied biomedical engineering from Johns Hopkins University, Baltimore, in 1995 and 2008, respectively.

Since 1986, he has been with the National Institute of Standards and Technology (NIST), Gaithersburg, MD, USA, where he was a Cooperative Education Student with the University of Maryland. During this time, he worked in the dc resistance area on the automation of resistance calibration systems. In 1991, he joined NIST as a full-time Electrical Engineer, working on the development of an automated ac resistance calibration system and the development of new resistance standards. Since 1994, he has been working in the high-resistance laboratory, developing automated measurement systems and improving standard resistors to support high-resistance calibration services and key comparisons. In recent years, he has worked on sensor technologies for the detection of biological molecules and low-current source and measure techniques. Since 2014, he has been leading the Metrology of the Ohm Project at NIST.